Loss of the cleaved-protamine 2 domain leads to incomplete histone-to-protamine exchange and infertility in mice

Lena Arévalo[1], Gina Esther Merges[1], Simon Schneider[1], Franka Enow Oben[1], Isabelle Neumann[1], Hubert Schorle[1]

[1] Department of Developmental Pathology, Institute of Pathology, University Hospital Bonn, Germany

Corresponding author: lena.arevalo@ukbonn.de, schorle@uni-bonn.de

Keywords: Protamines, PRM2 processing, chromatin, chromatin condensation, sperm, spermiogenesis, histone retention, protamine ratio

Abstract

Protamines are unique sperm-specific proteins that package and protect paternal chromatin until fertilization. A subset of mammalian species expresses two protamines (PRM1 and PRM2), while in others PRM1 is sufficient for sperm chromatin packaging. Alterations of the species-specific ratio between PRM1 and PRM2 are associated with infertility. Unlike PRM1, PRM2 is generated as a precursor protein consisting of a highly conserved N-terminal domain, termed cleaved PRM2 (cP2), which is consecutively trimmed off during chromatin condensation. The carboxyterminal part, called mature PRM2 (mP2), interacts with DNA and mediates chromatin-hypercondensation, together with PRM1. The removal of the cP2 domain is believed to be imperative for proper chromatin condensation and the prevention of DNA damage. Yet, the role of cP2 is not yet understood. Using CRISPR-Cas9 mediated gene editing, we generated mice lacking the cP2 domain while the mP2 is still expressed. We show that deletion of one allele of the cP2 domain is sufficient to render male mice infertile. cP2 deficient sperm show incomplete PRM2 incorporation, retention of transition proteins and a severely altered protamine ratio. During epididymal transit, cP2 deficient

sperm seem to undergo ROS mediated degradation leading to complete DNA fragmentation, inviability and immotility of mature sperm. The cP2 domain therefore seems to be necessary for the complex crosstalk leading to the successive and complete removal of transition proteins and complete protamination of sperm chromatin. Overall, we present the first step towards understanding the role of the cP2 domain in paternal chromatin packaging and open up avenues for further research.

Introduction

Chromatin structure and dynamics in the sperm nucleus are as unique as the sperm cell itself, and are of major importance to sperm function, fertilizing ability, and embryo survival. Paternal DNA is particularly vulnerable to damage, especially to oxidative stress during epididymal sperm maturation and migration, leading to a higher requirement for protection (Chen et al. 2002). At the same time, the size and shape of the sperm cell nucleus needs to be optimized for efficient sperm movement through the female reproductive tract (Tourmente et al. 2011). This is achieved by the complete reorganization of paternal chromatin from nucleo-histone to nucleo-protamine during the final steps of spermatogenesis (Balhorn 2007, Rathke et al. 2014).

Even though many studies have demonstrated that the correct execution of this transition is imperative for male fertility and embryo survival (Aoki and Carrell 2003), surprisingly little is known about the process itself. Recent studies have only just started to unravel its molecular basis (Schneider et al. 2016, Barral et al. 2017, Hada et al. 2017). Barral et al. (2017) were able to show that the testis specific histone variant H2A.L.2 together with TH2B and transition proteins (TNP1 and TNP2) mediates structural changes in chromatin allowing protamines to bind DNA. Protamines are small, arginine-rich proteins. Their high arginine content allows them to bind DNA with high affinity and to shield the charges of the DNA backbone more efficiently than histones (Balhorn 1989, Tanaka and Baba 2005). Two types of protamines have been identified in mammals: protamine 1 (*PRM1*, PRM1) and protamine 2 (*PRM2*, PRM2). While PRM1 is a major sperm protamine found across mammals, PRM2 is

57 only detected in the sperm of primates, most rodents, and a subset of other placental
58 mammals (Chauviere et al. 1992, Retief and Dixson 1993). The coding regions of *PRM1* and
59 *PRM2* are tightly clustered in a small section of chromosome 16 and it is highly likely that
60 *PRM2* is the result of a *PRM1* duplication event (Krawetz and Dixon 1988, Lüke et al. 2011).
61 Unlike PRM1, PRM2 is transcribed as a precursor. The N-terminal region of the translated
62 PRM2, termed cleaved-PRM2 (cP2), is successively cleaved over several days while
63 chromatin condensation is taking place. After this, only mature-PRM2 (mP2) remains bound
64 to the completely condensed DNA (Retief et al. 1993, Balhorn 2007, Yelick et al. 1987, Oliva
65 and Dixon 1991). Perturbations of PRM2 processing has been shown to lead to decreased
66 DNA integrity and sperm dysfunction (deYebra et al. 1998, Torregrosa et al. 2006). In
67 previous comparative evolutionary studies, it was shown that the cP2 coding sequence is
68 conserved in both primates and rodents. mP2, however, evolves under less selective
69 constraint (Lüke et al. 2011, 2016). Changes in coding sequences of cP2 were associated
70 with differences in sperm head size in mouse species. This association was specific to the
71 cP2 domain and not found for mP2 (Lüke et al. 2014a). A potential reason for this pattern is
72 that changes in cP2 are selected against conserving a crucial function for reproduction, while
73 mP2 is free to evolve under less constraint due to its proposed functional redundancy to
74 PRM1 (Lüke et al. 2011, 2016).
75 Proper PRM2 cleaving therefore seems to be crucial for successful reproduction, yet, the
76 function of the cP2 domain and PRM2 processing are unknown to date. Establishment and
77 analysis of PRM2 deficient mice revealed that $Prm2^{-/-}$ males were infertile, while $Prm2^{+/-}$
78 males remained fertile (Schneider et al. 2016). Of note mice deficient for TNP1, TNP2 and
79 H2A.L.2 display defects in PRM2 processing (PRM2 precursor detected in mature sperm
80 nuclei) (Yu et al. 2000, Zhao et al. 2001, Barral et al. 2017).
81 Given that cP2 cleaving is taking place during DNA condensation in late spermiogenesis, the
82 strong evolutionary conservation of this domain and the effect of incomplete PRM2
83 processing on sperm function and fertility, cP2 is likely to play an important role in the correct
84 execution of chromatin condensation. We therefore studied the involvement of cP2 in

85 chromatin condensation during spermiogenesis by generating and analyzing a mouse line
86 bearing a deletion of cP2, while maintaining mP2 expression (Prm2$^{\Delta c}$; MGI:6718282). We
87 analyzed fertility, testis and sperm morphology, chromatin integrity and nuclear protein
88 content of these mice and revealed that Prm2$^{\Delta c/+}$ mice are already infertile and that cP2
89 seems necessary for complete protamination of sperm chromatin.
90
91 **Material and Methods**
92 Animals
93 For the generation of mouse lines using CRISPR/Cas9 the F1 generation of mouse strains
94 C57Bl6 and DBA2 (B6D2F1) were used. Founder animals were backcrossed to C57Bl6.
95 Mice were maintained under standard laboratory conditions in environmentally controlled
96 rooms (20–24ºC) on a 12L:12D photoperiod with nesting material and ad libitum food and
97 water. All animal experiments were conducted according to German law of animal protection
98 and in agreement with the approval of the local institutional animal care committees
99 (Landesamt für Natur, Umwelt und Verbraucherschutz, North Rhine-Westphalia, Germany,
100 approval ID: AZ81-02.04.2018.A369, approved: 17.05.2019).
101
102 Gene-edited mouse lines
103 Guide RNA (gRNA) sequence pre-selection was performed using the algorithm published by
104 Hsu et al. (2013). Two gRNA sequences were selected based on quality scores in each case
105 maximizing specificity and minimizing off-target action (score > 50) (Table S1). The designed
106 guide sequences were ordered as crisprRNA sequences (crRNA) (IDT, Leuven, Belgium)
107 and annealed to tracrRNA (IDT) by incubating 5min at 95°C for a final concentration of 50mM
108 of gRNA (crRNA+tracrRNA). The target site of the designed gRNAs is shown in figure 1A.
109 The repair template used for homology directed repair (HDR), here single-stranded
110 oligodeoxynucleotides (ssODNs) (IDT) (Yoshimi et al. 2014, 2016), are shown in figure S1.
111 Ribonucleoprotein (RNP) complexes were assembled immediately prior to delivery by
112 incubation of 4pmol/µl Cas9 (IDT) protein, 4pmol/µl of each gRNA and 10pmol/µl ssODN in

113 Opti-MEM medium (Thermo Fisher Scientific, Waltham, USA) for 10min at room
114 temperature.
115 To generate gene-edited founder animals, B6D2F1 females were hormonally superovulated
116 and mated as described (Schneider et al. 2016). Oocytes were isolated from the
117 oviducts,washed and transferred into droplets of Opti-MEM medium containing the previously
118 prepared RNP complex and electroporated using a BioRad Gene Pulser (BioRad,
119 Feldkirchen, Germany) (two 3ms square wave pulses at 30V with an 100ms interval).
120 Oocytes were recovered and washed 5x in M2 medium (Merck Millipore, Darmstadt,
121 Germany) followed by 3 washes in KSOM (Merck Millipore) medium droplets. Oocytes were
122 then incubated in KSOM medium covered in paraffin oil overnight at 37°C. Developing 2-cell
123 stage embryos were then transferred into the oviducts of pseudo-pregnant foster mice.
124 Offspring was genotyped (primers, see Fig. 1A, Table S1) and positive founder animals
125 backcrossed to C57Bl/6J for at least 3 generations before analysis. Male mice between 10
126 and 13 weeks of age were used for analysis.
127
128 Fertility analysis
129 Five males per genotype were mated with C57Bl/6J females 1:2 and females were checked
130 daily for the presence of a vaginal plug until at least 5 plugs per male were observed.
131 Pregnancy rate and litter size were noted.
132
133 Sampling and mature sperm isolation
134 The testes were dissected and weighed. For paraffin sectioning, testes and epididymides
135 were fixed in either Bouin's solution for histology or in 4% Paraformaldehyde solution for
136 immunohistochemistry (IHC). For tubule preparations testes were transferred to PBS and
137 tubules dissected as described in Kotaja et al. (2004). Briefly, tubules were separated and
138 elongating and condensed spermatid containing sections were identified through their light
139 absorption pattern using a dissection microscope. Tubule sections were squashed on a slide,
140 frozen in liquid nitrogen for 20 seconds, fixed in 90% ethanol for 5 minutes and air dried.

141 Tubule preparations were used for IHC. To obtain sperm samples, caudae epididymes were
142 dissected and transferred to preheated (36-37°C) M2 medium, incised several times,
143 squeezed with tweezers several times during a 30min incubation period at 36-37°C to ensure
144 flushing out the whole sperm population including immotile sperm.
145
146 Histology
147 Bouin-fixed testes and epididymes were parraffized, embedded in paraffin blocks and
148 sectioned at 3 microns. Sections were deparaffinized and stained with the Periodic acid–
149 Schiff (PAS) procedure. Stained sections were imaged under bright field at 20x and 63x
150 magnification using a Leica DM5500 B microscope (Leica Microsystems, Wetzlar, Germany).
151
152 Basic sperm analysis
153 Isolated spermatozoa were counted for 6-12 animals per genotype using a hemocytometer.
154 Sperm motility was analyzed for 3-4 animals per genotype by taking 5-10, 3 second video
155 clips per animal using a Basler acA1920-155ucMED camera (Basler AG, Ahrensburg,
156 Germany). A minimum of 200 sperm per individual were analyzed and the percentage of
157 motile sperm calculated. Sperm viability was analyzed by eosin-nigrosin staining for 3-4
158 animals per genotype. Approximately 1 x 10^6 sperm were mixed with 50µl of eosin-nigrosin
159 dye, incubated for 30 seconds, spread on slides, air-dried and cover-slipped. A minimum of
160 200 spermatozoa were analyzed under bright field (Leica DMIRB microscope) and the
161 percentage of viable spermatozoa calculated.
162
163 RNAseq and differential expression analysis
164 RNA was extracted from testes after removal of the tunica albuginea using the RNeasy kit
165 (Qiagen, Hilden, Germany). RNA integrity (RIN) was determined using the RNA Nano 6000
166 Assay Kit with the Agilent Bioanalyzer 2100 system (Agilent Technologies, Santa Clara, CA,
167 USA). RIN values ranged from 7.3–10 for all samples. RNA sample quality control and library
168 preparation were performed by the University of Bonn Core facility for Next Generation

169 Sequencing (NGS), using the QuantSeq 3'-mRNA Library Prep (Lexogen, Greenland, NH,
170 USA). RNAseq was performed by the University of Bonn Core facility for Next Generation
171 Sequencing (NGS) on the Illumina HiSeq 2500 V4 platform, producing >10 million, 50bp 3'-
172 end reads per sample.
173 The samples were then mapped to the mouse genome (GRCm38.89) using HISAT2 2.1 (Kim
174 et al. 2015). StringTie 1.3.3 (Pertea et al. 2015) was used for transcript quantification and
175 annotation. Gene annotation was retrieved from the Ensembl FTP server
176 (ftp://ftp.ensembl.org)(GRCm38.89). The python script (preDE.py) included in the StringTie
177 package was used to prepare DEseq2-compatible gene-level count matrices for analysis of
178 differential gene expression. Mapping to the *Prm2* genomic location was visualized using the
179 Integrative Genomics Viewer (IGV; Robinson et al. 2011).
180 Differential expression (DE) was analyszed using DESeq2 1.16.1 (Love et al. 2014). The
181 adjusted p-value (Benjamini-Hochberg method) cutoff for DE was set at < 0.05, log2 fold
182 change of expression (LFC) cutoff was set at > 1. We performed GO term and pathway
183 overrepresentation analyses on relevant lists of genes using the PANTHER gene list analysis
184 tool with Fisher's exact test and FDR correction (Mi et al. 2017).
185
186 Sperm nuclear morphology
187 Nuclear morphology was analyzed for 3 individuals per genotype. Approximately 1.5 x 10^6
188 sperm were fixed in methanol-acetic acid (3:1), spread onto a slide and stained with 4′,6-
189 diamidino-2-phenylindole (DAPI) nuclear stain (ROTI®Mount FluorCare DAPI (Carl Roth
190 GmBH, Karlruhe, Germany)). At least 200 stained sperm cells per individual were imaged at
191 100x magnification using a Leica DM5500 B fluorescent microscope. Nuclear morphology
192 was analyzed using the stand-alone version of the Nuclear Morphology program by Skinner
193 et al. (2019). The program allows for automated detection and morphological analysis of
194 mouse sperm nuclei (among other species and cell types). It additionally provides options for
195 clustering heterogenous populations by nuclear parameters and comparative analyses of

196 nuclear morphology (Skinner et al. 2019). The parameters used for nucleus detection are
197 shown in figure S3.
198
199 Sperm basic nuclear protein extraction and analysis
200 Basic nuclear proteins were extracted described in Soler-Ventura et al. (2018). Briefly,
201 approximately 10 x 10^6 of swim-out sperm were washed in PBS and pelleted. The pellet was
202 resuspended in buffer containing 1M Tris pH 8, 0.5M MgCl and 5ul Triton X-100.
203 Subsequently the pellet was treated with 1mM PMSF in water inducing cell lysis. Treatment
204 with EDTA, DTT and GuHCl induced DNA denaturation. Incubation at 37°C for 30min in
205 presence of 0.8% vinylpyridine is necessary for mouse protamine separation on the
206 subsequent protein gel. DNA is then precipitated by addition of EtOH and separated from the
207 sample by centrifugation. Basic sperm nuclear proteins are then extracted and dissolved in
208 0.5M HCl, followed by protein precipitation with TCA, acetone washes and drying. The
209 precipitated proteins are resuspended in sample buffer containing 5.5 M urea, 20% β-
210 mercapto-ethanol and 5% acetic acid.
211 The samples were then run on a pre-electrophorized acid-urea polyacrylamide gel (AU-
212 PAGE) (2.5 M urea, 0.9 M acetic acid, and 15% acrylamide/0.1% N,N′-Methylene bis-
213 acrylamide, TEMED and APS). The extracted basic nuclear proteins migrate towards the
214 negative pole at a 150V for 1h, 50min. The gels were stained with Coomassie Brilliant Blue
215 (Sigma Aldrich, Taufkirchen, Germany) using standard procedures. The two main protamine
216 bands can be observed in the bottom of the gel with mature-PRM2 corresponding to the
217 upper and PRM1 the lower band (Ishibashi et al. 2010, Soler-Ventura et al. 2018). PRM2
218 precursor bands can be observed in the lower part of the gel above the mature-PRM2 band,
219 if present (Yu et al. 2000, de Mateo et al. 2011). In the upper half of the gel, bands
220 corresponding to other basic nuclear proteins, including histones can be found (see Soler-
221 Ventura 2018). The densities of Coomassie stained bands were analyzed using ImageJ
222 (1.52k, Schneider et al. 2012).
223

224 Immunohistochemistry

225 PFA fixed testis and epididymis sections as well as EtOH fixed tubule preparations were
226 used for immunofluorescent staining. Sections were deparaffinized in xylol and rehydrated.
227 Sections and tubule preparations were washed in PBS and blocked for 30 min with normal
228 horse serum (Vectorlabs, Burlingame, USA) at room temperature, followed by primary
229 antibody incubation over night at 4°C. Antibodies and dilutions are shown in table S3. Slides
230 were then double-stained with fluorescent secondary antibodies using the VectaFluor™ Duet
231 Immunofluorescence Double Labeling Kit, DyLight® 594 Anti-Rabbit (red), DyLight® 488
232 Anti-Mouse (green) (Vectorlabs, Burlingame, USA), DAPI counterstained and coverslipped
233 with ProLong™ Gold antifade reagent with DAPI (Thermo Fisher Scientific, Waltham, USA).
234

235 Mass spectrometry and differential protein abundance analysis

236 Basic nuclear protein extractions were done for 3 individuals per genotype using
237 approximately 10^6 sperm. Extracted proteins were dissolved in sample buffer (5.5 M urea,
238 20% β-mercapto-ethanol and 5% acetic acid).
239 Peptide preparation: Protein solutions (5.5 M urea, 20% 2-mercaptoethanol, 5% acetic acid)
240 were dried in a vacuum concentrator and subjected to in solution preparation of peptides.
241 Proteins were dissolved in 50 mM acrylamide solution (Tris-HCl, pH=8) and alkylated for 30
242 min at RT. 1 µg of Trypsin were added for o/n proteolysis at 37°C. Dried peptides were
243 dissolved in 10 µL 0.1% trifluoro acetic acid (TFA) and desalted with ZipTips (Waters GmbH,
244 Eschborn, Germany) according to standard solid-phase extraction procedures. Equilibration
245 and binding was done in presence of 0.1% TFA, washing with 0.1% formic acid (FA). Eluates
246 (50% acetonitrile, 0.1% FA) were dried and stored at -20°C.
247 LC-MS measurements: Peptide separation was performed on a Dionex Ultimate 3000 RSLC
248 nano HPLC system (Dionex GmbH, Idstein, Germany). The autosampler was operated in µl-
249 pickup mode. Peptides were dissolved in 10 µl 0.1% FA (solvent A). 2 µL were injected onto
250 a C18 analytical column (300 mm length, 75 µm inner diameter, ReproSil-Pur 120 C18-AQ,
251 1.9 µm). Peptides were separated during a linear gradient from 2% to 35% solvent B (90%

252 acetonitrile, 0.1% FA) within 90 min at 300 nl/min. The nanoHPLC was coupled online to an
253 Orbitrap Fusion Lumos mass spectrometer (Thermo Fisher Scientific, Bremen, Germany).
254 Peptide ions between 300 and 1600 m/z were scanned in the Orbitrap detector every 3
255 seconds with R=120,000 (maximum fill time 50 ms, AGC target 400,000). Polysiloxane
256 (445.12002 Da) was used for internal calibration (typical mass error ≤1.5 ppm). In a top-
257 speed method peptides were subjected to higher energy collision induced dissociation (HCD:
258 1.0 Da isolation, threshold intensity 25,000, normalized energy 27%) and fragments analyzed
259 in the Orbitrap with target 50,000 and maximum injection time 22 ms, R=15,000. Fragmented
260 peptide ions were excluded from repeat analysis for 20 s.
261 Data analysis: Raw data processing and was performed with Proteome Discoverer software
262 2.5.0.400 (Thermo Fisher Scientific). Peptide identification was done with an in-house
263 Mascot server version 2.6.1 (Matrix Science Ltd, London, UK). MS data were searched
264 against *Mus musculus* sequences from SwissProt (2021/03, including isoforms), and
265 contaminants (cRAP, Mellacheruvu et al. 2013). Precursor Ion m/z tolerance was 10 ppm,
266 fragment ion tolerance 20 ppm. Tryptic peptides with up to two missed cleavages were
267 searched. Propionamide on cysteines was set as static modification. Oxidation was allowed
268 as dynamic modification of methionine, acetylation as modification of protein N-termini.
269 Mascot results were evaluated by the percolator algorithm (Kall et al. 2008) version 3.05 as
270 implemented in Proteome Discoverer. Spectra with identifications below 1% q-value were
271 sent to a second round of database search with semitryptic enzyme specificity (one missed
272 cleavage allowed). Protein N-terminal acetylation, methionine oxidation, carbamylation on
273 lysine and N-termini were allowed as dynamic modifications. Actual FDR values were
274 typically ≤0.5% (peptide spectrum matches), ≤1.0% (peptides), <1% (proteins). Proteins were
275 accepted if at least two peptides with q-value <1% were identified. Summed abundances
276 (areas of precursor extracted ion chromatograms of unique peptides) were used for relative
277 quantification.
278 Differential abundance (DA) analysis: DA analysis was performed using the Bioconductor
279 package proDA (Ahlmann-Eltze C 2021) using peptide spectrum matches (PSM) level data

280 extracted from Protein Discoverer. Only proteins detected in all genotypes and all replicates
281 with more than two peptides were included in the analysis. The data were log2 transformed
282 and median normalized prior to DA analysis to ensure comparability. The proDA package is
283 based on linear models and utilized Bayesian priors to increase power for differential
284 abundance detection (Ahlmann-Eltze C 2021). Proteins with a log2 fold change (LFC) of >1
285 and false discovery rate adjusted p-value (FDR) <0.05 were considered differentially
286 abundant compared to the WT. Plots were generated using the R-package ggplot2 (Wickam
287 2016).
288
289 Generation of expression plasmids and transfection
290 *Prm2* and Prm2$^{\Delta c}$ cDNA (GenBank: NM_008933.2) was amplified from C57Bl6 mouse testis
291 cDNA using overhang primers introducing suitable restriction enzyme motifs (table S1) and
292 cloned N-terminally in-frame with eGFP into the pEGFP-N3 vector (6080-1). Correct
293 sequence and insertion were verified by sequencing.
294 Human Embryonic Kidney 293 (HEK293) cells were cultured in standard medium (DMEM,
295 10% FBS). HEK293 cells were transfected at 80% confluence with 3 µg of pPrm2-EGFP-N3
296 (*Prm2*), pPrm2$^{\Delta c}$-EGFP-N3 (Prm2$^{\Delta c}$ sequence) or pEGFP-N3 with FuGENE® HD
297 Transfection Reagent (Promega, Madison, USA), according to the manufacturer's
298 instructions. At 12 hours post-transfection the medium was changed. Pictures were taken
299 after 48 hours using a Leica DMIRB inverted microscope (Leica Microsystems, Wetzlar,
300 Germany).
301
302 **Results**
303 Generation of gene-edited mouse lines
304 To delete cP2 in the reading frame of the PRM2 gene, we used CRISPR/Cas9 with
305 templates inducing homology directed repair (HDR). In order to induce the deletion we used
306 two gRNAs targeting the 5' and 3' ends of the cP2 domain (Fig. 1A). A single stranded DNA
307 template encoding the 5' and 3' areas flanking the cP2 coding region enabling an in-frame

308 repair of the Prm2$^{\Delta c}$ allele was added to the gene-editing reaction (Fig. S1). The sequence of
309 the generated allele, named Prm2$^{\Delta c}$, is shown in figure 1A. The allele was registered with
310 mouse genomics database (MGI:6718282). Animals were generated, sequence validated
311 and backcrossed to C57Bl/6J for at least 3 generations before analysis.
312
313 Prm2$^{\Delta c/+}$ as well as Prm2$^{\Delta c/-}$ male mice are infertile
314 First, we subjected the Prm2$^{\Delta c/+}$ mice to a fertility test. Five Prm2$^{\Delta c/+}$ male mice were mated to
315 ten WT females and the pregnancy/litters were recorded for five confirmed vaginal plugs per
316 male (successful matings). We found that Prm2$^{\Delta c/+}$ male mice were infertile, with no observed
317 pregnancies in at least five confirmed matings each. This is in contrast to the deletion of the
318 entire PRM2 gene, where Prm2$^{+/-}$ male mice remained fertile (Schneider et al. 2016) (Fig.
319 1B). We hypothesized that an aberrant interaction between mP2 and the PRM2 precursor
320 expressed from the wildtype allele might lead to interference and be causative for infertility in
321 these males. In order to test this, we crossed Prm2$^{\Delta c/+}$ females with Prm2$^{+/-}$ males published
322 by us (Prm2$^{\Delta 97bp}$; Schneider et al. 2016, MGI:5760133) to generate Prm2$^{\Delta c/-}$ mice. This
323 results in male mice, in which, only Prm2$^{\Delta c}$ is present and expressed. However, Prm2$^{\Delta c/-}$
324 males did not produce any litters in at least five confirmed matings each and can be
325 considered infertile (Fig. 1B). This strongly suggests, that the cP2 domain is essential for
326 murine spermiogenesis. If cP2 was non-essential these Prm2$^{\Delta c/-}$mice should be fertile, similar
327 to Prm2$^{+/-}$ males.
328
329 mP2 is expressed in Prm2$^{\Delta c/-}$ mice and transcriptional silencing does not seem to be
330 disrupted
331 Since the Prm2$^{\Delta c/-}$ allows for detection of mP2 transcripts from the Prm2$^{\Delta c}$ allele we decided
332 to perform RNAseq on testis samples and analyze expression of *Prm2* transcripts. By
333 visualizing the RNAseq read mapping to the *Prm2* genomic location, we were able to
334 demonstrate that the mP2 domain was indeed expressed (Fig. 1C, Fig. S2). The expression

335 level of the mP2 domain does not differ from WT levels in Prm2$^{\Delta c/+}$ or Prm2$^{\Delta c/-}$, thus the
336 alleles do not display a gene dosage effect (Fig. 1D).
337 In our previous study we found that in the Prm2$^{-/-}$ testis, a much higher number of genes was
338 differentially higher than lower expressed (81:13) indicating incomplete protamine-mediated
339 transcriptional silencing (Schneider et al. 2020). Here, compared to WT we found 36 genes
340 differentially higher expressed and 42 genes differentially lower expressed for Prm2$^{\Delta c/+}$ males
341 and 26 genes differentially higher and 43 differentially lower for Prm2$^{\Delta c/-}$ (Fig. 1E). This
342 indicates that transcriptional silencing is not notably disrupted in males harbouring the
343 Prm2$^{\Delta c}$ allele. Nine genes were found to be differentially expressed in both Prm2$^{\Delta c/+}$ and
344 Prm2$^{\Delta c/-}$ males. No GO-term or pathway enrichment was found for the analyzed gene sets.
345 Of note, *Pcgf5* (polycomb group ring finger 5) is higher expressed in both Prm2$^{\Delta c/+}$ and
346 Prm2$^{\Delta c/-}$ males. *Pcgf5* is part of the Polycomb repressive complex 1 (PRC1) mediating
347 heritable histone modifications. It is important for X-inactivation and can activate transcription
348 when forcibly recruited into chromatin (Piunti and Shilatifard 2021). Lists of differentially
349 expressed genes and statistics can be found in supplementary dataset S1.
350
351 <u>mP2 is expressed and mP2 protein condenses DNA in Prm2$^{\Delta c/+}$ and Prm2$^{\Delta c/-}$ male mice, but</u>
352 <u>is also found in condensing spermatid cytoplasm and residual bodies</u>
353 After confirming, that the gene-edited mP2-domain is expressed from the Prm2$^{\Delta c}$ allele we
354 next addressed the question, whether mP2 can be detected in spermatids and is able to
355 condense DNA. We therefore first performed IHC on PFA fixed testis sections. The epitope
356 of the PRM2 antibody (Hup2B, Briarpatch Bio, Livermore, USA) is located in the first half of
357 the mP2 domain and is able to detect both, the PRM2 protein generated from the wildtype
358 and the gene-edited Prm2$^{\Delta c}$ allele. As shown in figure 2A, PRM2 is detected in condensed
359 spermatid nuclei of Prm2$^{\Delta c/+}$ and Prm2$^{\Delta c/-}$ males, similar to the wildtype. However, we
360 additionally detected a signal in the cytoplasm of spermatids and residual bodies that is
361 strongest in Prm2$^{\Delta c/-}$ males and not found in wildtype (Fig. 2A).

362 To determine if mP2 is able to condense DNA, we expressed PRM2 and the mP2 sequence
363 of the Prm2$^{\Delta c}$ allele tagged with eGFP in HEK293 cells. The ability of PRM1 to bind to DNA
364 and condense nuclei when expressed *in vitro* in somatic cells had been demonstrated before
365 by Iuso et al. (2015) in sheep fibroblasts. Experiments revealed that PRM2-eGFP and
366 Prm2$^{\Delta c}$-eGFP locate to the HEK293 cell nuclei and are present after 48h as large speckles in
367 the nucleus (Fig. 2B) respectively. We therefore concluded that mP2 is able to condense the
368 nucleus of somatic cells *in vitro* and should therefore be able to contribute to spermatid
369 chromatin condensation *in vivo*.
370
371 Testis histology is inconspicuous, while mature sperm are inviable and immotile in Prm2$^{\Delta c/+}$
372 and Prm2$^{\Delta c/-}$ male mice
373 Next, we analyzed testis mass and examined histological sections to determine the nature of
374 the infertility. Relative testes mass did not differ from the wildtype (Fig. 3A). Almost no viable
375 and motile mature sperm were found in Prm2$^{\Delta c/+}$ and Prm2$^{\Delta c/-}$ males (Mean percent viable:
376 Prm2$^{\Delta c/+}$=1.7, SD=1.31; Prm2$^{\Delta c/-}$=0; Mean percent motile: Prm2$^{\Delta c/+}$=0.2, SD=0.45; Prm2$^{\Delta c/-}$
377 =0.25, SD=0.5) (Fig. 3A, Fig. S4). Interestingly, sperm count is significantly reduced in
378 Prm2$^{\Delta c/-}$ but not in Prm2$^{\Delta c/+}$ males compared to the wildtype (ANOVA: $F(2)=10.87$, $p<0.001$;
379 Post-hoc Tukey HSD: WT vs. Prm2$^{\Delta c/+}$: $p=0.89$, WT vs. Prm2$^{\Delta c/-}$: $p<0.001$) (Fig. 3A). To
380 determine if the loss of cP2 affects spermiogenesis, testis and epididymis histology was
381 evaluated by PAS staining of Bouin-fixed sections. Testis histology was inconspicuous and
382 spermatogenesis seemed not to be affected in either genotype (Fig. 3B). Epididymis
383 histology however, shows larger round cells, vacuole-like structures which are indicative of
384 spermatid degradation. This was more pronounced in Prm2$^{\Delta c/-}$ males compared to Prm2$^{\Delta c/+}$
385 males (Fig. 3B).
386
387 Chromatin integrity is strongly affected and nuclear morphology is altered in Prm2$^{\Delta c/+}$ and
388 Prm2$^{\Delta c/-}$ male mice.

389 Since protamines condense sperm chromatin, and were shown to influence sperm head
390 morphology (Lüke et al. 2014a,b), mature sperm DNA integrity and nuclear morphology
391 could be affected even though mP2 is able to condense DNA. We therefore extracted DNA
392 from mature sperm and subjected it to agarose gel electrophoresis. In DNA from sperm of
393 Prm2$^{\Delta c/+}$ males DNA is completely fragmented (Fig. 4A). Schneider et al. (2020) was able to
394 show that during epididymal transit, Prm2$^{-/-}$ deficient sperm underwent ROS mediated
395 destruction, leading to DNA and membrane degradation and immotility. We therefore stained
396 sections of epidydimes against 8-Oxo-2'-deoxyguanosine (8-OHdG), which indicates
397 oxidative DNA damage. In the caput epididymis we detected only a slight increase of the 8-
398 OHdG signal in Prm2$^{\Delta c/+}$ and Prm2$^{\Delta c/-}$ males compared to the wildtype. However, in the
399 Prm2$^{\Delta c/+}$cauda epididymis a strong increase in 8-OHdG was visible compared to the wildtype.
400 The 8-OHdG signal in the Prm2$^{\Delta c/-}$ cauda was less intense, which is likely due to the more
401 severe degradation and reduced sperm count (Fig. 4B).
402 Nuclear morphology analysis revealed aberrant nuclear morphology of mature sperm in
403 Prm2$^{\Delta c/+}$ and Prm2$^{\Delta c/-}$ males. Sperm from both genotypes show a significantly reduced
404 nuclear size compared to the WT (Table S2, Fig. 4C, Fig. S5). Prm2$^{\Delta c/+}$ males show two
405 clusters of nuclear shape, a slimmer nucleus with decreased hook curvature and a smaller
406 hookless nucleus. This phenotype is similar but more severe in Prm2$^{\Delta c/-}$ males (Table S2,
407 Fig. 4C, Fig. S5). Of note nuclear morphology of Prm2$^{\Delta c/-}$ and Prm2$^{\Delta c/+}$ deficient sperm also
408 differs from Prm2$^{+/-}$ and Prm2$^{-/-}$ males.
409
410 <u>The protamine ratio is flipped in Prm2$^{\Delta c/+}$ and Prm2$^{\Delta c/-}$ males</u>
411 Since the ratio between PRM1 and PRM2 is constant in mature sperm (in mice ~60%
412 PRM2), and alterations of this ratio are associated with sperm defects and infertility (Corzett
413 et al. 2002, Steger et al. 2008; García-Peiró et al. 2011), we next wanted to test if male mice
414 harbouring the Prm2$^{\Delta c}$ allele display alterations of the PRM1/PRM2 ratio. Interestingly, acid-
415 urea gel electrophoresis (AU-PAGE) of mature sperm basic nuclear proteins showed several
416 bands corresponding to PRM2 precursors in Prm2$^{\Delta c/+}$ males. This was also the case in

417 Prm2$^{+/-}$ males. Through analyzing the densities of the PRM1 band relative to mP2 and PRM2
418 precursor bands, we found the PRM ratio to be strongly altered, showing a lower percentage
419 of PRM2 (including precursors) compared to the wildtype in Prm2$^{\Delta c/+}$ and Prm2$^{\Delta c/-}$ males
420 (Mean %PRM2: WT=69,29; Prm2$^{\Delta c/+}$=42,07; Prm2$^{\Delta c/-}$=26.78)(ANOVA: F(2)=18.98,p=0.009;
421 Post-hoc Tukey HSD: WT vs. Prm2$^{\Delta c/+}$: p=0.04, WT vs. Prm2$^{\Delta c/-}$: p=0.008). This does not
422 seem to be the case in Prm2$^{+/-}$ males, for which we find the percentage of PRM2 (including
423 precursors) to be similar to the wildtype (%PRM2=66.57 (n=1)) (Fig. 4C, Fig. S7).
424
425 Histone-to-protamine transition is incomplete in Prm2$^{\Delta c/+}$ and Prm2$^{\Delta c/-}$ males
426 Since we found the protamine ratio to be altered and PRM2 seemed aberrantly located in the
427 cytoplasm and residual bodies of condensing/condensed spermatids in the testis, we next
428 evaluated the histone-to-protamine transition. To this end, we performed IHC staining to
429 detect histone H3, transition protein 1 (TNP1) and PRM1 in testis and epididymis sections. in
430 Prm2$^{\Delta c/+}$, PRM1 staining intensity and localization is comparable to the WT. However, PRM1
431 staining seems to be lost in Prm2$^{\Delta c/-}$ sperm from cauda epididymis (Fig. S6, Fig. 5). This
432 might be due to the strong degradation of the sperm and its DNA and low sperm count in this
433 genotype. We did not find any apparent increase in total histone H3 signal (Fig. S6, Fig. 5),
434 However, TNP1 was retained in both Prm2$^{\Delta c/+}$ and Prm2$^{\Delta c/-}$ males in step 15-16 spermatids
435 and caput epididymal sperm. In cauda epididymal sperm however, we did not find any visible
436 signal of TNP1 (Fig. S6, Fig. 5).
437 In order to further investigate histone retention and alteration in nuclear protein content we
438 performed mass spectrometric analysis on mature sperm basic nuclear protein extracts and
439 analyzed differential abundance (DA) of the detected proteins. Compared to wildtype, we
440 found 14 proteins to be DA in Prm2$^{\Delta c/+}$ sperm, 20 in Prm2$^{\Delta c/-}$ males and 24 for Prm2$^{-/-}$ sperm.
441 Seven proteins were DA in all three comparisons, several of those associated with stress
442 response and/or apoptosis (HSPA2, B2M, CLU) (Fig. 6A,B). Consistent with IHC results we
443 did not find any histones that were significantly higher abundant in Prm2$^{\Delta c/+}$ or Prm2$^{\Delta c/-}$ males.
444 We therefore conclude that histone retention is not increased in males harbouring the Prm2$^{\Delta c}$

445 allele. Interestingly in the Prm2$^{-/-}$ samples we did find histones (H3f3, H3C, H4C),
446 significantly higher abundant, indicating increased histone retention when PRM2 is
447 completely lacking. TNPs were not detected. Lists of DA proteins including statistics can be
448 found in supplementary dataset S2.
449 Eight proteins were not DA in Prm2$^{-/-}$ compared to WT, but in Prm2$^{\Delta c/+}$ and/or Prm2$^{\Delta c/-}$ males.
450 Of these, RPL26 and GSTM5 are involved in DNA damage response and/or oxidative stress
451 pathways, while TUBA3B and ANT4 (*Slc25a31*) are related to motility. Of note, citrate
452 synthase (CS) is specifically higher abundant in Prm2$^{\Delta c/+}$ and Prm2$^{\Delta c/-}$ males. Most
453 interestingly, we found the histone H2A variant H2A.L.2 to be significantly lower abundant in
454 Prm2$^{\Delta c/-}$ males, compared to the wildtype (Fig. 6A-D). H2A.L.2 is a spermatid/sperm-specific
455 histone variant and a key player in histone-to-protamine transition. Together with TH2B it
456 forms a nucleosome with an open chromatin structure allowing for loading of transition
457 proteins followed by protamine recruitment and histone and transition protein eviction by
458 protamines (Barral et al. 2017) (Fig. 6D). According to Hoghoughi et al. (2020) H2A.L.2 is
459 retained in mature sperm in pericentric heterochromatin. We therefore investigated the
460 presence and co-localization of H2A.L.2 and PRM2 in Prm2$^{\Delta c/-}$ and Prm2$^{\Delta c/+}$ males, by
461 immunofluorescent staining of condensed step 15-16 spermatids from tubule preparations
462 and mature sperm extracted from the cauda epididymis. As expected, in the wildtype, we
463 found a moderately strong signal for H2A.L.2 in the pericentric region of the nucleus, with
464 PRM2 signal in the whole nucleus (Fig. 7). Interestingly, we see only a weak signal in the
465 pericentric region of mature sperm but a stronger signal in the nuclear region close to the
466 neck, which also shows strong DAPI signal (Fig. 7). However, in Prm2$^{\Delta c/+}$ and Prm2$^{\Delta c/-}$
467 spermatids the H2A.L.2 signal is stronger and localized in solid, almost clumped foci in the
468 nucleus that correspond to the strongest DAPI signal. In mature sperm, however, the
469 H2A.L.2 signal is almost completely lost, consistent with the lower abundance found in the
470 mass spectrometric analysis. The PRM2 signal is diffuse and distributed along the whole
471 mature sperm cell, likely due to severe membrane damage and degradation (Fig. 7).
472

473 **Discussion**

474 The crucial role of protamines in the process of sperm chromatin reorganization is well
475 known. However, why two protamines are needed in some species, while PRM1 seems to be
476 sufficient in others is still unclear. The main difference between PRM1 and PRM2 is the
477 highly conserved N-terminal cleaved PRM2 domain (cP2). Its function remains elusive to
478 date. By understanding its role in chromatin condensation, we can shed light on the
479 necessity for two protamines and the importance of the protamine ratio (Aoki et al. 2006, de
480 Mateo et al. 2009, Zatecka et al. 2014). Here we show that the cP2 domain is indispensable
481 for PRM2 function and necessary for male mouse fertility. Mice heterozygous for the deletion
482 of the domain display inviable and immotile sperm. Loss of the cP2 leads to an perturbation
483 of the transition proteins eviction and incorporation of PRM2. While overall histone retention
484 is not increased, the histone variant H2A.L.2 is less abundant in mature sperm deficient in
485 cP2.

486 Firstly, mP2 expressed from the Prm2$^{\Delta c}$ allele was detected in the nucleus of
487 condensed spermatids of cP2 deficient mice and was shown to be able to condense somatic
488 cell DNA *in-vitro* similar to PRM2, or PRM1 (Iuso et al. 2015). We therefore conclude that the
489 mP2 domain seems to maintain its main function during spermiogenesis in cP2 deficient
490 mouse lines. Male Prm2$^{\Delta c/+}$ mice are infertile, show complete fragmentation of mature sperm
491 DNA, loss of viability and immotility of mature sperm. We hypothesized that this could be due
492 to an aberrant interaction between mP2 and the PRM2 precursor. If this was the case, male
493 mice should be fertile if the full-length PRM2 was not expressed. Similarly, if cP2 was non-
494 essential these mice should be fertile, just as Prm2$^{+/-}$ males. We therefore bred the Prm2$^{\Delta c}$
495 allele with the Prm2$^{\Delta 97bp}$ mouse line (Schneider et al. 2016, MGI:5760133) generated and
496 analyzed by Schneider et al. (2016, 2020). However, mice expressing only mP2 (Prm2$^{\Delta c/-}$)
497 were also infertile showing an even more extreme phenotype than heterozygous males. cP2
498 therefore seems to be essential for male fertility in mice.

499 Since mature sperm chromatin is completely fragmented in cP2 deficient males and
500 mature sperm are inviable and immotile similar to Prm2$^{-/-}$ sperm, we suspected that sperm

501 might undergo epididymal degradation mediated by oxidative stress. Schneider et al. (2020)
502 showed that loss of PRM2 seems to lead to reduced antioxidant capacity of sperm, initiating
503 an oxidative stress-mediated destruction cascade during epididymal transit. Indeed, cP2
504 deficient mice showed a strong increase in oxidative DNA damage in the cauda epididymis.
505 Prm2$^{\Delta c/-}$ sperm seem to be degraded to an extent that many of the caudal sperm are
506 completely disintegrated, leading to a significantly reduced sperm count. We propose that
507 this is not a specific effect of cP2 or PRM2 deficiency but an inherent epididymal mechanism
508 evoked by DNA damage or aberrant protamination (or even otherwise damaged sperm, e.g.:
509 membrane defects, aberrant morphology or sperm surface proteome). How sperm damage
510 might be sensed by epididymal cells and what, in fact, initiates this cascade is an interesting
511 avenue for further investigation.

512 Given the timing of *Prm2* expression and processing, the primary effects of cP2 loss
513 are likely to be found during the transition from histone-bound to protaminized DNA in the
514 final stages of spermiogenesis. Barral et al. (2017) describe this transition taking place by
515 assembly of a histone (TH2B and H2A.L.2) - transition protein (TNP1 and TNP2) interface
516 followed by protamine recruitment and processing. Protamines themselves subsequently
517 replace histones. This process is disrupted in cP2 deficient mice. Firstly, cP2 deficient mice
518 show a strong amount of mP2 in the cytoplasm and residual bodies in addition to the signal
519 found in the nucleus, indicating that mP2 is not completely incorporated into the condensing
520 chromatin. Incidentally, this seems to lead to a switch in protamine ratio, which is around 2:1
521 in wildtype but 1:2-1:5 in cP2 deficient sperm. Secondly, we found retention of TNP1 in
522 condensed testicular spermatids and caput epididymal sperm, indicating that mP2 might not
523 be able to evict TNP1 efficiently or that TNP1 is binding DNA in a competitive manner.
524 Surprisingly, however, histone retention was not increased. This was confirmed by H3
525 immunostaining and mature sperm basic nuclear protein abundance analysis. Thus, it seems
526 loss of cP2 specifically affects the removal of transition proteins. Interestingly, we do find an
527 increased retention of H3 and H4 variants in Prm2$^{-/-}$ deficient sperm. Additionally, a recent
528 study investigating a single residue mutation in PRM1 showed increased histone retention,

529 but no transition protein retention in such mice (Moritz et al. 2021). We therefore propose
530 that cP2 is important for correct interaction between PRM2 and transition proteins and
531 replacement of transition proteins by PRM2. Transition proteins are believed to aid in
532 chromatin condensation by stabilizing the DNA in a non-supercoiled state, cooperating with
533 topoisomerases to relieve torsional stress and to be involved in DNA repair during chromatin
534 condensation (Singh and Rao, 1988 Lèvesque et al. 1998, Akama et al. 1999). Loss of either
535 transition protein results in incomplete PRM2 processing (Yu et al. 2000, Shirley et al. 2004)
536 and TNP2 was shown to interact with PRM2 (Barral et al. 2017). In order to investigate if
537 mP2 is in fact unable to replace transition proteins, in-vitro assays in somatic cell culture
538 could give valuable insights.

539 The transition protein retention we found in cP2 deficient mice seems to go along with
540 seemingly aberrant retention of H2A.L.2 in condensed spermatids which is lost in mature
541 sperm, where in fact H2A.L.2 is lower abundant compared to the wildtype. Thus, the H2A.L.2
542 – transition protein complexes seem to be first retained and then lost during epididymal
543 transit. During the first steps of chromatin condensation H2A.L.2, together with TH2B
544 provides an open chromatin interface necessary for transition protein loading. KO of H2A.L.2
545 leads to infertility, aberrant transition protein loading and processing of PRM2 (Barral et al.
546 2017). In mature sperm H2A.L.2 was shown to be retained in pericentric heterochromatin
547 (Govin et al. 2007, Hoghoughi et al. 2020). This retention seems to be lost in $Prm2^{\Delta c/-}$ mature
548 sperm. A pericentric localization can still be observed in $Prm2^{\Delta c/-}$condensed spermatids. Yet,
549 the strong signal we find in condensed spermatids overlaps with speckles of strong DAPI
550 signal. We therefore propose that the H2A.L.2-transition protein complexes might be retained
551 in clumps of hypercondensed chromatin. Protamines have a strong electrostatic attraction to
552 DNA due to arginine clusters (Moritz et al. 2021). This allows protamines to condense DNA
553 even in the absence of spermatid specific histones and transition proteins, as shown in *in-*
554 *vitro* assays in somatic cells and in this study (Iuso et al. 2015). However, uncontrolled or
555 unbalanced binding of protamines might lead to strong torsional stress and DNA damage. A
556 controlled stepwise chromatin condensation therefore could be required to maintain

557 chromatin integrity. Moritz et al. (2021) recently showed that the PRM2 precursor has a lower
558 DNA binding affinity than mP2, leading to faster DNA condensation by mP2. Barral et al.
559 (2017) suggested that transition proteins buffer protamine incorporation by allowing for
560 ordered protamine loading and (or possibly through) PRM2 processing. By losing the cP2
561 domain this processing step is skipped. We therefore propose, as a working hypothesis for
562 further investigation, that the aberrant interaction with transition proteins due to cP2
563 deficiency leads to random mP2 binding, leading to strong hypercondensation of open
564 chromatin resulting in DNA strand breaks. Transition protein-loaded chromatin, however
565 does not allow for mP2 loading, leading to incomplete mP2 incorporation and H2A.L.2 –
566 transition protein retention that is lost by DNA degradation during epididymal transit.
567 In conclusion, our results show that the cleaved domain of PRM2 is essential for
568 sperm function and fertility. Loss of the domain leads to incomplete protamination, a switch in
569 the protamine ratio and transition protein retention in epididymal sperm. During epididymal
570 transit cP2 deficient sperm are degraded, seemingly by ROS mediated damage, leading to
571 complete DNA fragmentation. cP2 seems to be necessary for correct interaction between the
572 H2A.L.2 - transition protein complex and PRM2. We were able to provide a first glimpse into
573 the function of cleaved PRM2 and PRM2 processing, that opens up multiple avenues for
574 further investigation.
575
576 **Acknowledgments:** This study was supported by a grant from the Deutsche
577 Forschungsgemeinschaft (DFG) to L.A. (AR 1221/1-1). L.A. was further supported by the
578 University of Bonn Medical school supplementary research grant program *FEMHABIL.* We
579 thank Gaby Beine, Angela Egert and Andrea Jäger for excellent technical assistance. Protein
580 identifications were done at the Core Facility Mass Spectrometry, Institute of Biochemistry
581 and Molecular Biology, Medical Faculty, University of Bonn. Mass spectrometer funded by
582 the Deutsche Forschungsgemeinschaft (DFG) – Projektnummer 386936527. RNAseq was
583 done at University of Bonn Core facility for Next Generation Sequencing (NGS). We thank
584 Saddi Khochbin and Sophie Barral for the gift of the H2A.L.2 antibody and excellent advice.

585

586 **Author contributions:** L.A. and H.S. conceived the study and designed the experiments.
587 L.A. and S.S. generated gene-edited mice. L.A. and G.E.M. analysed gene-edited mice.
588 F.E.O. and I.N. generated IHC stainings. L.A. and H.S. drafted the manuscript. All authors
589 read and approved the final manuscript.

590

591 **References**

592 Ahlmann-Eltze C, Anders S. proDA: Probabilistic dropout analysis for identifying differentially
593 abundant proteins in label-free mass spectrometry. Biorxiv. 2020; 1:661496.
594 Akama K, Kondo M, Sato H, Nakano M. Transition protein 4 from boar late spermatid nuclei
595 is a topological factor that stimulates DNA-relaxing activity of topoisomerase I. FEBS
596 letters. 1999; 442:189-92.
597 Aoki VW, Liu L, Jones KP, Hatasaka HH, Gibson M, Peterson CM, Carrell DT. Sperm
598 protamine 1/protamine 2 ratios are related to in vitro fertilization pregnancy rates and
599 predictive of fertilization ability. Fertility and Sterility. 2006; 86:1408-15.
600 Balhorn R. Mammalian Proteins: structure and Molecular Interaction. In: Adolph KW, editor.
601 Molecular Biology of Chromosome Function. New York: Springer Verlag; 1989. pp. 366–
602 395.
603 Balhorn R. The protamine family of sperm nuclear proteins. Genome Biol. 2007; 227.
604 doi:10.1186/gb-2007-8-9-227
605 Barral S, Morozumi Y, Tanaka H, Montellier E, Govin J, de Dieuleveult M, et al. Histone
606 Variant H2A.L.2 Guides Transition Protein-Dependent Protamine Assembly in Male Germ
607 Cells. Mol Cell. 2017; 89–101.e8. doi:10.1016/j.molcel.2017.02.025
608 Chauviere M, Martinge A, DeBarle M, Sautiere P, Chevallier P. Molecular characterization of
609 six intermediate proteins in the processing of mouse protamine P2 precursor. Eur J
610 Biochem. 1992; 759–765. doi:10.1111/j.1432-1033.1992.tb16691.x

611 Chen H, Cheung MPL, Chow PH, Cheung ALM, Liu W, O WS. Protection of sperm DNA
612 against oxidative stress in vivo by accessory sex gland secretions in male hamsters.
613 Reproduction. 2002; 491–499.
614 Corzett M, Mazrimas J, Balhorn R. Protamine 1: Protamine 2 stoichiometry in the sperm of
615 eutherian mammals. Mol Reprod Dev. 2002; 519–527. doi:10.1002/mrd.10105
616 de Mateo S, Gázquez C, Guimerà M, Balasch J, Meistrich ML, Ballescà JL, Oliva R.
617 Protamine 2 precursors (Pre-P2), protamine 1 to protamine 2 ratio (P1/P2), and assisted
618 reproduction outcome. Fertility and sterility. 2009; 91:715-22.
619 de Mateo S, Ramos L, de Boer P, Meistrich M, Oliva R. Protamine 2 precursors and
620 processing. Protein and peptide letters. 2011; 18:778-85.
621 de Yebra L, Ballescá JL, Vanrell JA, Corzett M, Balhorn R, Oliva R. Detection of P2
622 precursors in the sperm cells of infertile patients who have reduced protamine P2 levels.
623 Fertil Steril. 1998; 755–9.
624 García-Peiró A, Martínez-Heredia J, Oliver-Bonet M, Abad C, Amengual MJ, Navarro J,
625 Jones C, Coward K, Gosálvez J, Benet J. Protamine 1 to protamine 2 ratio correlates with
626 dynamic aspects of DNA fragmentation in human sperm. Fertility and sterility. 2011;
627 95:105-9.
628 Govin J, Escoffier E, Rousseaux S, Kuhn L, Ferro M, Thévenon J, Catena R, Davidson I,
629 Garin J, Khochbin S, Caron C. Pericentric heterochromatin reprogramming by new
630 histone variants during mouse spermiogenesis. The Journal of cell biology. 2007;
631 176:283-94.
632 Hada M, Masuda K, Yamaguchi K, Shirahige K, Okada Y. Identification of a variant-specific
633 phosphorylation of TH2A during spermiogenesis. Sci Rep. 2017; 46228.
634 doi:10.1038/srep46228
635 Hoghoughi N, Barral S, Curtet S, Chuffart F, Charbonnier G, Puthier D, Buchou T,
636 Rousseaux S, Khochbin S. RNA-Guided genomic localization of H2A. L. 2 histone variant.
637 Cells. 2020; 9:474.

638 Ishibashi T, Li A, Eirín-López JM, Zhao M, Missiaen K, Abbott DW, Meistrich M, Hendzel MJ,
639 Ausio J. H2A. Bbd: an X-chromosome-encoded histone involved in mammalian
640 spermiogenesis. Nucleic acids research. 2010; 38:1780-9.
641 Iuso D, Czernik M, Toschi P, Fidanza A, Zacchini F, Feil R, Curtet S, Buchou T, Shiota H,
642 Khochbin S, Ptak GE. Exogenous expression of human protamine 1 (hPrm1) remodels
643 fibroblast nuclei into spermatid-like structures. Cell reports. 2015; 13:1765-71.
644 Käll L, Storey JD, MacCoss MJ, Noble WS. Assigning significance to peptides identified by
645 tandem mass spectrometry using decoy databases. Journal of proteome research. 2008;
646 7:29-34.
647 Kim D, Langmead B, Salzberg S L. HISAT: A fast spliced aligner with low memory
648 requirements. Nat Methods. 2015; 12:357–360.
649 Kotaja N, Kimmins S, Brancorsini S, Hentsch D, Vonesch JL, Davidson I, Parvinen M,
650 Sassone-Corsi P. Preparation, isolation and characterization of stage-specific
651 spermatogenic cells for cellular and molecular analysis. Nature methods. 2004;1:249-54.
652 Krawetz SA, Dixon GH. Sequence similarities of the protamine genes: Implications for
653 regulation and evolution. J Mol Evol. 1988; 291–297. doi:10.1007/BF02101190
654 Lévesque D, Veilleux S, Caron N, Boissonneault G. Architectural DNA-binding properties of
655 the spermatidal transition proteins 1 and 2. Biochemical and biophysical research
656 communications. 1998; 252:602-9.
657 Love M I, Huber W, Anders S. 2014. Moderated estimation of fold change and dispersion for
658 RNA-seq data with DESeq2. Genome Biol. 2014; 15:1–21.
659 Lüke L, Campbell P, Varea Sánchez M, Nachman MW, Roldan ERS. Sexual selection on
660 protamine and transition nuclear protein expression in mouse species. Proc Biol Sci.
661 2014; 20133359. doi:10.1098/rspb.2013.3359
662 Lüke L, Tourmente M, Roldan ERS. Sexual selection of protamine 1 in mammals. Mol Biol
663 Evol. 2016; 174–184. doi:10.1093/molbev/msv209

664 Lüke L, Vicens A, Serra F, Luque-Larena JJ, Dopazo H, Roldan ERS, et al. Sexual Selection
665 Halts the Relaxation of Protamine 2 among Rodents. PLoS One. 2011; e29247.
666 doi:10.1371/journal.pone.0029247
667 Lüke L, Vicens A, Tourmente M, Roldan ERS. Evolution of protamine genes and changes in
668 sperm head phenotype in rodents. Biol Reprod. 2014; 67.
669 doi:10.1095/biolreprod.113.115956
670 Mellacheruvu D, Wright Z, Couzens AL, Lambert JP, St-Denis NA, Li T, Miteva YV, Hauri S,
671 Sardiu ME, Low TY, Halim VA. The CRAPome: a contaminant repository for affinity
672 purification–mass spectrometry data. Nature methods. 2013; 10:730-6.
673 Mi H, Huang X, Muruganujan A, Tang H, Mills C, Kang D, Thomas PD. 2017. PANTHER
674 version 11: Expanded annotation data from Gene Ontology and Reactome pathways, and
675 data analysis tool enhancements. Nucleic Acids Res. 2017; 45:D183–D189.
676 Moritz L, Schon S, Rabbani M, Sheng Y, Pendlebury D, Agrawal R, Sultan C, Jorgensen K,
677 Zheng X, Diehl A, Ragunathan K. Single residue substitution in protamine 1 disrupts
678 sperm genome packaging and embryonic development in mice. bioRxiv. 2021.
679 Oliva R, Dixon GH. Vertebrate protamine genes and the histone-to-protamine replacement
680 reaction. Biology WEC and KMBT-P in NAR and M, editor. Prog Nucleic Acid Res Mol
681 Biol; 1991; 25–94.
682 Pertea M, Pertea GM, Antonescu CM, Chang TC, Mendell JT, Salzberg SL. 2015. StringTie
683 enables improved reconstruction of a transcriptome from RNA-seq reads. Nat Biotechnol.
684 2015; 33:290–295.
685 Piunti A, Shilatifard A. The roles of Polycomb repressive complexes in mammalian
686 development and cancer. Nature Reviews Molecular Cell Biology. 2021; 22:326-45.
687 Rathke C, Baarends WM, Awe S, Renkawitz-Pohl R. Chromatin dynamics during
688 spermiogenesis. Biochimica et Biophysica Acta - Gene Regulatory Mechanisms. 2014;
689 155–168. doi:10.1016/j.bbagrm.2013.08.004
690 Retief JD, Dixon GH. Evolution of pro-protamine P2 genes in primates. Eur J Biochem. 1993;
691 609–615. doi:10.1111/j.1432-1033.1993.tb17960.x

692 Retief JD, Winkfein RJ, Dixon GH, Adroer R, Queralt R, Ballabriga J, et al. Evolution of
693 Protamine P1 Genes in Primates. J Mol Evol. 1993; 426–434.
694 Robinson JT, Thorvaldsdóttir H, Winckler W, Guttman M, Lander ES, Getz G, Mesirov JP.
695 Integrative genomics viewer. Nature biotechnology. 2011; 29:24-6.
696 Ruiz-Lopez MJ, Espeso G, Evenson DP, Roldan ERS, Gomendio M. Paternal levels of DNA
697 damage in spermatozoa and maternal parity influence offspring mortality in an
698 endangered ungulate. Proc R Soc B Biol Sci. 2010; 2541–2546.
699 doi:10.1098/rspb.2010.0333
700 Schneider et al 2020Schneider S, Shakeri F, Trötschel C, Arévalo L, Kruse A, Buness A,
701 Poetsch A, Steger K, Schorle H. Protamine-2 deficiency initiates a reactive oxygen
702 species (ROS)-mediated destruction cascade during epididymal sperm maturation in
703 mice. Cells. 2020; 9:1789.
704 Schneider S, Balbach M, Jan F. Jikeli, Fietz D, Nettersheim D, Jostes S, et al. Re-visiting the
705 Protamine-2 locus: deletion, but not haploinsufficiency, renders male mice infertile. Sci
706 Rep. 2016; 36764. doi:10.1038/srep36764
707 Shirley CR, Hayashi S, Mounsey S, Yanagimachi R, Meistrich ML. Abnormalities and
708 reduced reproductive potential of sperm from Tnp1-and Tnp2-null double mutant mice.
709 Biology of reproduction. 2004;71:1220-9.
710 Singh J, Rao MRS. Interaction of rat testis protein, TP, with nucleosome core particle.
711 Biochem Int. 1988; 17:701–710
712 Skinner BM, Rathje CC, Bacon J, Johnson EE, Larson EL, Kopania EE, Good JM, Yousafzai
713 G, Affara NA, Ellis PJ. A high-throughput method for unbiased quantitation and
714 categorization of nuclear morphology. Biology of reproduction. 2019; 100:1250-60.
715 Soler-Ventura A, Castillo J, de la Iglesia A, Jodar M, Barrachina F, Ballesca JL, Oliva R.
716 Mammalian sperm protamine extraction and analysis: a step-by-step detailed protocol and
717 brief review of protamine alterations. Protein and peptide letters. 2018; 25:424-33.
718 Steger K, Wilhelm J, Konrad L, Stalf T, Greb R, Diemer T, Kliesch S, Bergmann M, Weidner
719 W. Both protamine-1 to protamine-2 mRNA ratio and Bcl2 mRNA content in testicular

720 spermatids and ejaculated spermatozoa discriminate between fertile and infertile men.
721 Human Reproduction. 2008; 23:11-6.
722 Tanaka H, Baba T. Gene expression in spermiogenesis. Cell Mol Life Sci. 2005; 344–354.
723 doi:10.1007/s00018-004-4394-y
724 Torregrosa N, Domínguez-Fandos D, Camejo MI, Shirley CR, Meistrich ML, Ballescà JL, et
725 al. Protamine 2 precursors, protamine 1/protamine 2 ratio, DNA integrity and other sperm
726 parameters in infertile patients. Hum Reprod. 2006; 2084–9. doi:10.1093/humrep/del114
727 Tourmente M, Gomendio M, Roldan ERS. Sperm competition and the evolution of sperm
728 design in mammals. BMC Evol Biol. 2011; 12. doi:10.1186/1471-2148-11-12
729 Wickham H. ggplot2. Wiley Interdisciplinary Reviews: Computational Statistics. 2011; 3:180-
730 5.
731 Yelick P, Balhorn ROD, Johnson PA, Corzett M, Mazrimas JOEA, Kleene KKC, et al. Mouse
732 protamine 2 is synthesized as a precursor whereas mouse protamine 1 is not. Mol Cell
733 Biol. Am Soc Microbiol; 1987; 2173. doi:10.1128/MCB.7.6.2173.
734 Yu YE, Zhang Y, Unni E, Shirley CR, Deng JM, Russell LD, Weil MM, Behringer RR,
735 Meistrich ML. Abnormal spermatogenesis and reduced fertility in transition nuclear protein
736 1-deficient mice. Proceedings of the National Academy of Sciences. 2000; 97:4683-8.
737 Zatecka E, Castillo J, Elzeinova F, Kubatova A, Ded L, Peknicova J, Oliva R. The effect of
738 tetrabromobisphenol A on protamine content and DNA integrity in mouse spermatozoa.
739 Andrology. 2014; 2:910-7.
740 Zhao M, Shirley CRCR, Yu YEE, Mohapatra B, Zhang YUN, Unni E, et al. Targeted
741 disruption of the transition protein 2 gene affects sperm chromatin structure and reduces
742 fertility in mice. Mol Cell Biol. 2001; 7243. doi:10.1128/MCB.21.21.7243
743

744 **Figure legends**

745 **Figure 1.** Gene editing, fertility and expression. A) Schematic representation of the
746 generation of cP2 deletion. Gene-edited coding sequence and predicted translation are
747 shown. B) Schematic overview of analyzed genotypes and fertility. $Prm2^{+/-}$ and $Prm2^{-/-}$

748 (Schneider et al. 2016) were included as a comparison. Barplot of average litter size for WT,
749 Prm2$^{+/-}$, Prm2$^{-/-}$, Prm2$^{\Delta c/+}$ and Prm2$^{\Delta c/-}$, n=5 for each genotype. C) Representative section of
750 *Prm2* RNAseq read mapping for WT, Prm2$^{\Delta c/+}$ and Prm2$^{\Delta c/-}$. Visualized using Integrative
751 Genomics Viewer (IGV; Robinson et al. 2011). D) Barplot showing average DESeq2
752 normalized read counts of *Prm2* for WT, Prm2$^{\Delta c/+}$ and Prm2$^{\Delta c/-}$. E) Barplot showing
753 comparison between number of differentially higher and lower expressed genes for Prm2$^{\Delta c/+}$
754 and Prm2$^{\Delta c/-}$ compared to wildtype.
755
756 **Figure 2.** Localization and DNA condensing ability of mP2. A) Immunohistochemical
757 fluorescent staining of PRM2 (WT, Prm2$^{\Delta c/+}$) or mP2 (Prm2$^{\Delta c/+}$, Prm2$^{\Delta c/-}$) (green) in testis
758 sections, counterstaining with DAPI (blue). Scale bar = 50µm. B) Heterologous expression of
759 plasmids encoding eGFP tagged PRM2 (*Prm2*-eGFP) or mP2 (*mP2*-eGFP) in human
760 embryonic kidney 293 (HEK) cells 48 hours post-transfection. Scale bar = 10µm.
761
762
763 **Figure 3.** Sperm and testis parameters and histology. A) Barplots showing data for relative
764 testes mass, mature sperm count, percentage of viable mature sperm (eosin-nigrosin assay)
765 and percentage of motile mature sperm in Prm2$^{\Delta c/+}$ and Prm2$^{\Delta c/-}$ mice compared to wildtype.
766 B) PAS staining of testis and epididymal sections of Prm2$^{\Delta c/+}$, Prm2$^{\Delta c/-}$ and WT males. Scale
767 bar = 50µm (200µm for left column).
768
769 **Figure 4.** Chromatin integrity, nuclear morphology and protamine content. A) Agarose gel of
770 DNA extracted from WT, Prm2$^{+/-}$, Prm2$^{-/-}$ and Prm2$^{\Delta c/+}$ mature sperm. B)
771 Immunohistochemical fluorescent staining of 8-Oxo-2'-deoxyguanosine (8-OHdG) (green) in
772 caput epididymis (upper row) and cauda epididymis (lower row) of Prm2$^{\Delta c/+}$, Prm2$^{\Delta c/-}$ and WT.
773 Counterstained with DAPI (pseudo-colored grey). Scale bar = 50µm. C) Comparison of
774 mature sperm nucleus consensus shapes of WT, Prm2$^{+/-}$, Prm2$^{-/-}$, Prm2$^{\Delta c/+}$ and Prm2$^{\Delta c/-}$
775 resulting from nuclear morphology analysis. Numbers inside the consensus shapes indicate

776 the number of nuclei assessed and assigned to the respective consensus shape cluster.
777 Upper row shows the consensus shape of the different gene edited lines overlaid with the
778 wildtype consensus shape. cl. = cluster. D) Representative lanes of acid-urea gel
779 electrophoresis (AU-PAGE) of WT, Prm2$^{+/-}$, Prm2$^{-/-}$, Prm2$^{\Delta c/+}$ and Prm2$^{\Delta c/-}$ mature sperm
780 basic nuclear protein extractions. a=non-protamine basic nuclear proteins, b=PRM2
781 precursors, open arrowhead indicates mature PRM2 band, solid arrowhead indicates PRM1
782 band. To the right: quantification of the percentage of PRM2 (including PRM2 precursors) of
783 total protamine by band density analysis. Asterisk indicates significant difference.
784
785 **Figure 5.** Histone H3, transition protein 1 and protamine 1 staining. Two left columns:
786 Immunohistochemical fluorescent staining of Histone H3 (H3) (red) and protamine 1 (PRM1)
787 (green) in WT, Prm2$^{\Delta/+}$ and Prm2$^{\Delta/-}$ caput epididymis. Counterstained with DAPI (blue). Scale
788 bar = 50µm. Columns to the right: Immunohistochemical fluorescent staining of transition
789 protein 1 (TNP1) (red) and protamine 1 (PRM1) (green) in WT, Prm2$^{\Delta/+}$ and Prm2$^{\Delta/-}$ caput
790 and cauda epididymis. Counterstained with DAPI (blue). Scale bar = 50µm.
791
792 **Figure 6.** Differential abundance of mature sperm basic nuclear proteins. A) volcano plots
793 showing differential abundance (DA) of basic nuclear proteins in Prm2$^{\Delta/+}$ compared to WT
794 (upper plot) and Prm2$^{\Delta/-}$ compared to WT (lower plot). Significantly DA proteins are indicated
795 in color (teal = lower abundant, yellow = higher abundant). Top DA proteins and proteins of
796 interest are labeled with their corresponding gene symbol. B) Venn diagram showing the
797 overlap between DA proteins found in the three different comparisons (WT vs. Prm2$^{\Delta/+}$, WT
798 vs. Prm2$^{\Delta/-}$ and WT vs. Prm2$^{-/-}$). Proteins present in overlaps of interest are listed with their
799 corresponding gene symbol. H2A.L.2 is marked in red. C) Boxplot of median normalized log2
800 abundance of H2A.L.2 in WT, Prm2$^{-/-}$, Prm2$^{\Delta/+}$ and Prm2$^{\Delta/-}$. D) Interaction network for
801 H2A.L.2 extracted from String database (Szklarczyk et al. 2019).
802

803 **Figure 7.** Immunohistochemical staining of H2A.L.2 and PRM2. Immunohistochemical
804 fluorescent staining of H2A.L.2 (red) and PRM2 (green) in WT, $Prm2^{\Delta/+}$ and $Prm2^{\Delta/-}$ step 15-
805 16 spermatids from tubule preparations (two left columns) and mature sperm extracted from
806 cauda epididymis (two right columns). Counterstained with DAPI (blue). Scale bar = 20μm.

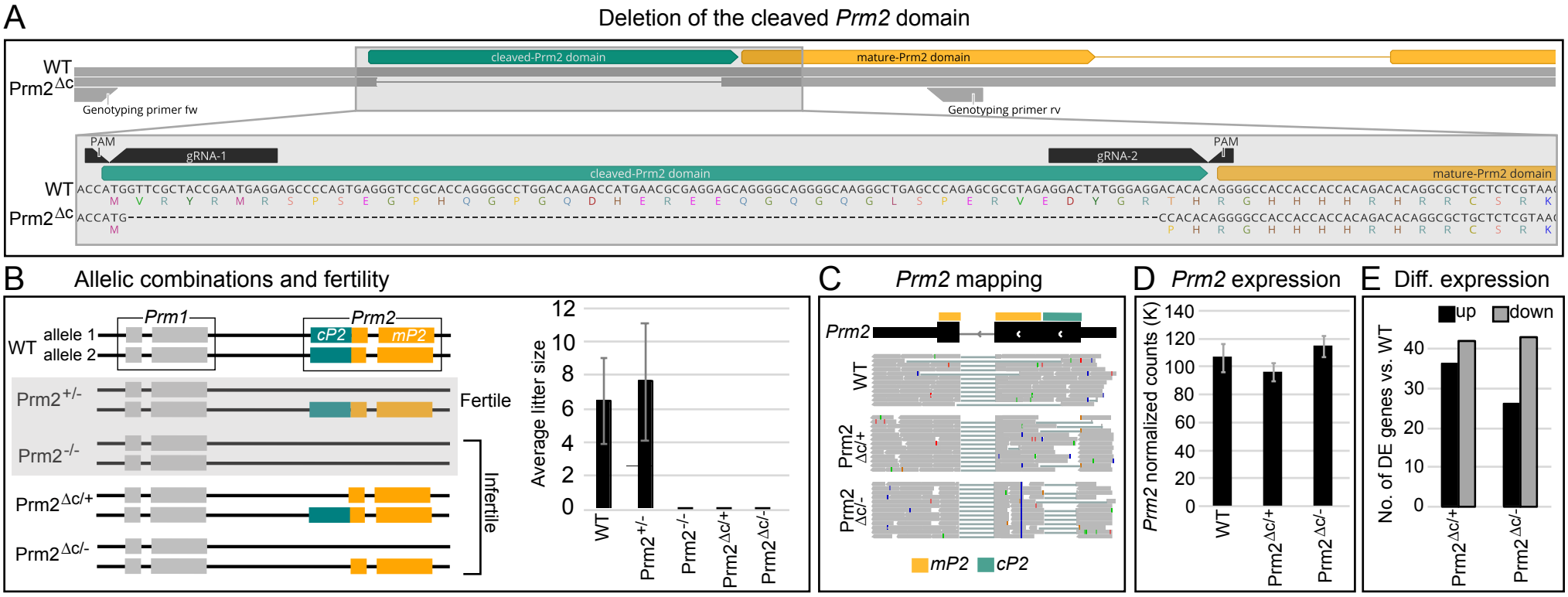
A
Deletion of the cleaved Prm2 domain
WT
Prm2Δc
cleaved-Prm2 domain
mature-Prm2 domain
Genotyping primer fw
Genotyping primer rv
PAM
gRNA-1
gRNA-2
PAM
cleaved-Prm2 domain
mature-Prm2 domain
WT ACCATGGTTCGCTACCGAATGAGGAGCCCCAGTGAGGGTCCGCACCAGGGGCCTGGACAAGACCATGAACGCGAGGAGCAGGGGCAGGGGCAAGGGCTGAGCCCAGAGCGCGTAGAGGACTATGGGAGGACACACAGGGGCCACCACCACCACAGACACAGGCGCTGCTCTCGTAA
M V R Y R M R S P S E G P H Q G P G Q D H E R E E Q G Q G Q G L S P E R V E D Y G R T H R G H H H H R H R R C S R K
Prm2Δc ACCATG----------CCACACAGGGGCCACCACCACCACAGACACAGGCGCTGCTCTCGTAA
M P H R G H H H H R H R R C S R K
B
Allelic combinations and fertility
Prm1
Prm2
cP2
mP2
WT allele 1
allele 2
Prm2+/-
Fertile
Prm2-/-
Prm2Δc/+
Prm2Δc/-
Infertile
Average litter size
12
10
8
6
4
2
0
WT
Prm2+/-
Prm2-/-
Prm2Δc/+
Prm2Δc/-
C
Prm2 mapping
Prm2
WT
Prm2 Δc/+
Prm2 Δc/-
mP2
cP2
D
Prm2 expression
Prm2 normalized counts (K)
140
120
100
80
60
40
20
0
WT
Prm2Δc/+
Prm2Δc/-
E
Diff. expression
up
down
No. of DE genes vs. WT
40
30
20
10
0
Prm2Δc/+
Prm2Δc/-

Fig. 1

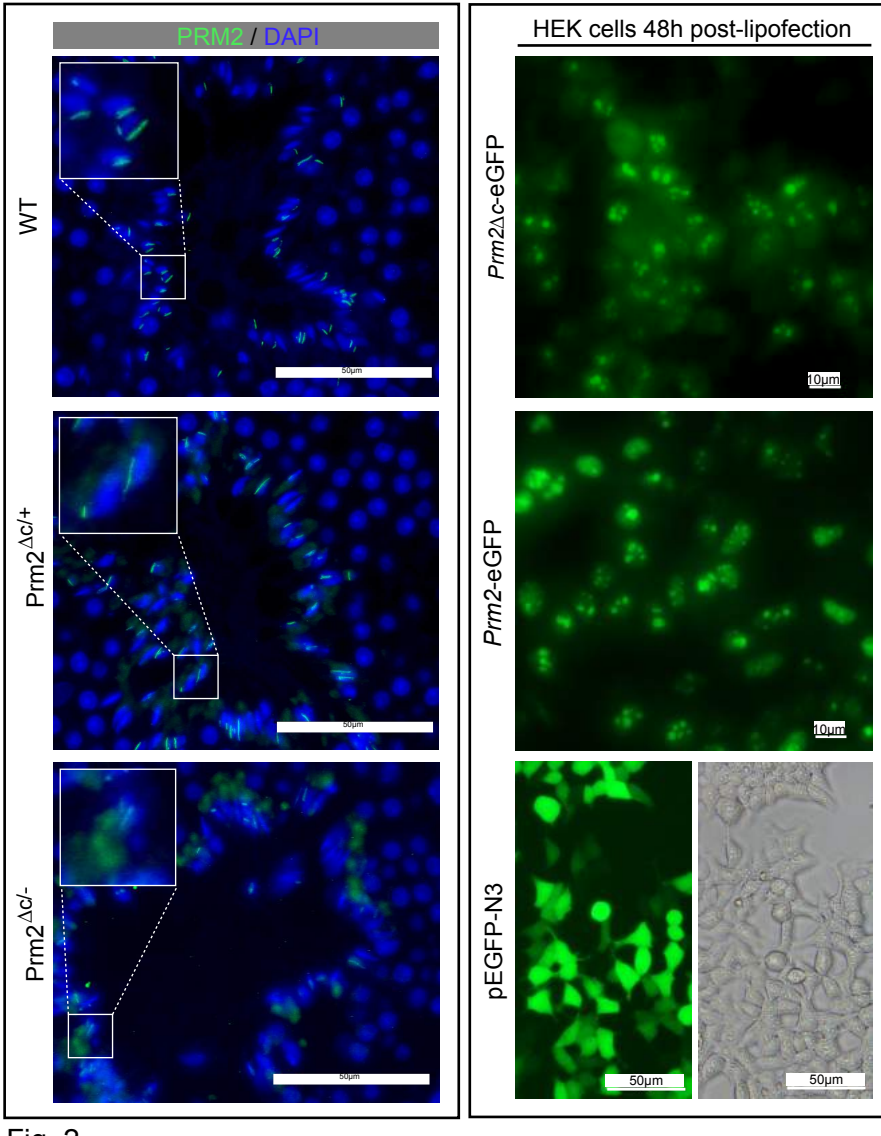
A
IHC (Step 15-16 spermatids)
PRM2 / DAPI
WT
Prm2Δc/+
Prm2Δc/-
50µm
B
Heterologous expression
HEK cells 48h post-lipofection
Prm2Δc-eGFP
Prm2-eGFP
pEGFP-N3
10µm
50µm

Fig. 2

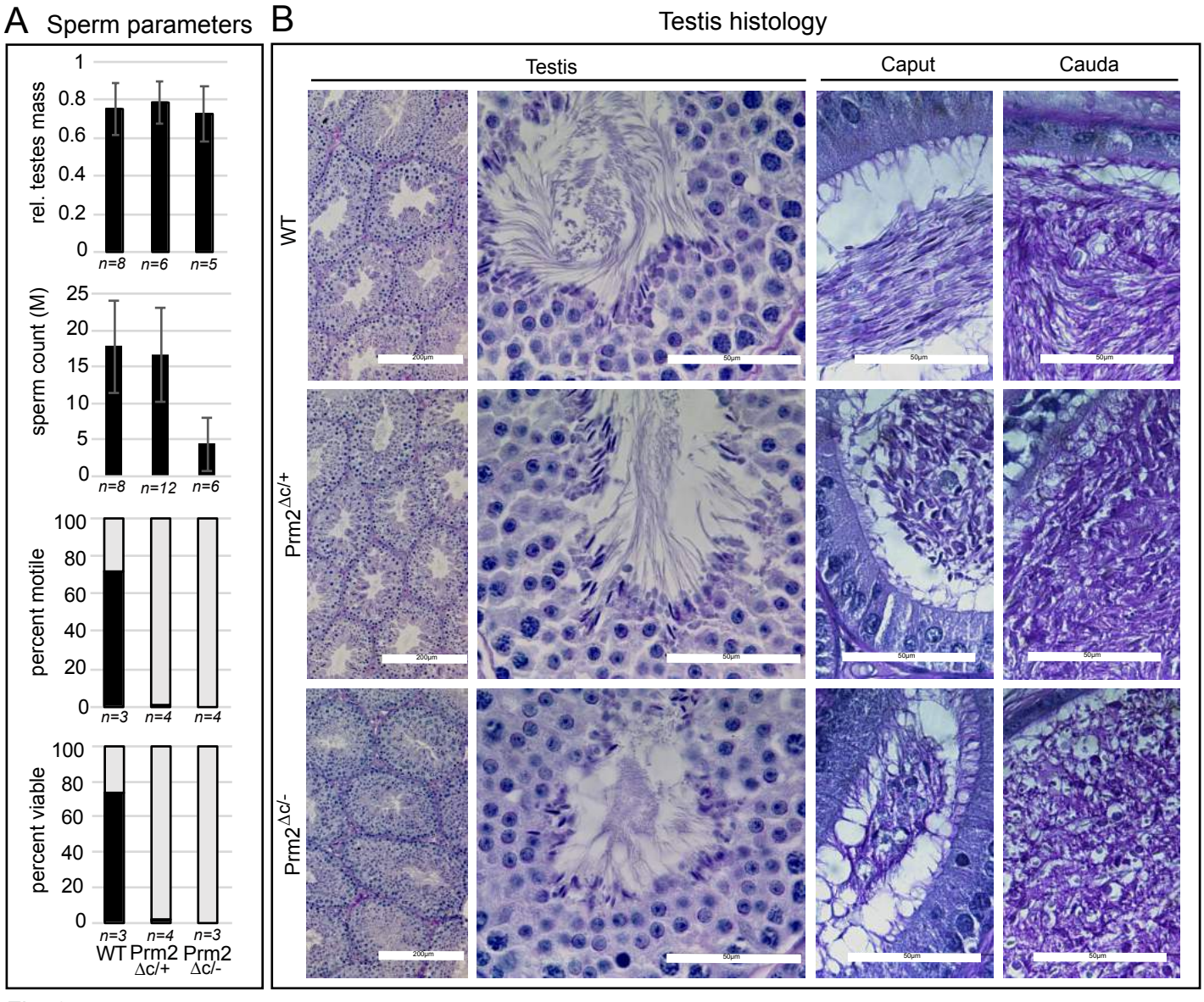
A
Sperm parameters
rel. testes mass
1
0.8
0.6
0.4
0.2
0
n=8
n=6
n=5
sperm count (M)
25
20
15
10
5
0
n=8
n=12
n=6
percent motile
100
80
60
40
20
0
n=3
n=4
n=4
percent viable
100
80
60
40
20
0
n=3
n=4
n=3
WT
Prm2 Δc/+
Prm2 Δc/-
B
Testis histology
Testis
Caput
Cauda
WT
Prm2Δc/+
Prm2Δc/-
200µm
50µm

Fig. 3

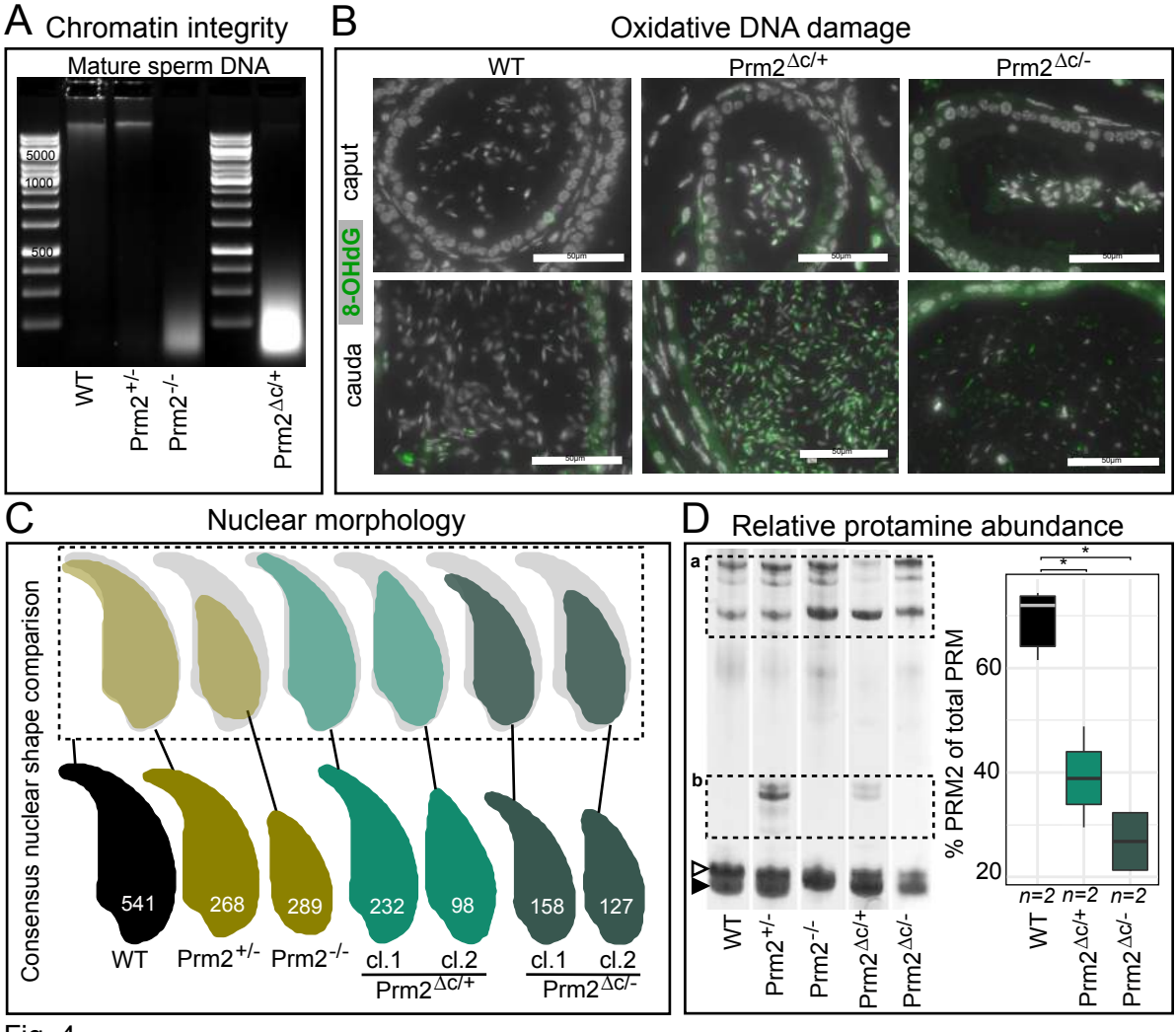
A Chromatin integrity
Mature sperm DNA
5000
1000
500
WT
Prm2+/-
Prm2-/-
Prm2Δc/+
B Oxidative DNA damage
WT
Prm2Δc/+
Prm2Δc/-
caput
8-OHdG
cauda
50µm
C Nuclear morphology
Consensus nuclear shape comparison
541
268
289
232
98
158
127
WT
Prm2+/-
Prm2-/-
cl.1
cl.2
Prm2Δc/+
cl.1
cl.2
Prm2Δc/-
D Relative protamine abundance
a
b
WT
Prm2+/-
Prm2-/-
Prm2Δc/+
Prm2Δc/-
% PRM2 of total PRM
60
40
20
*
*
n=2
n=2
n=2
WT
Prm2Δc/+
Prm2Δc/-

Fig. 4

Histone H3, Transition protein 1 and Protamine 1 IHC

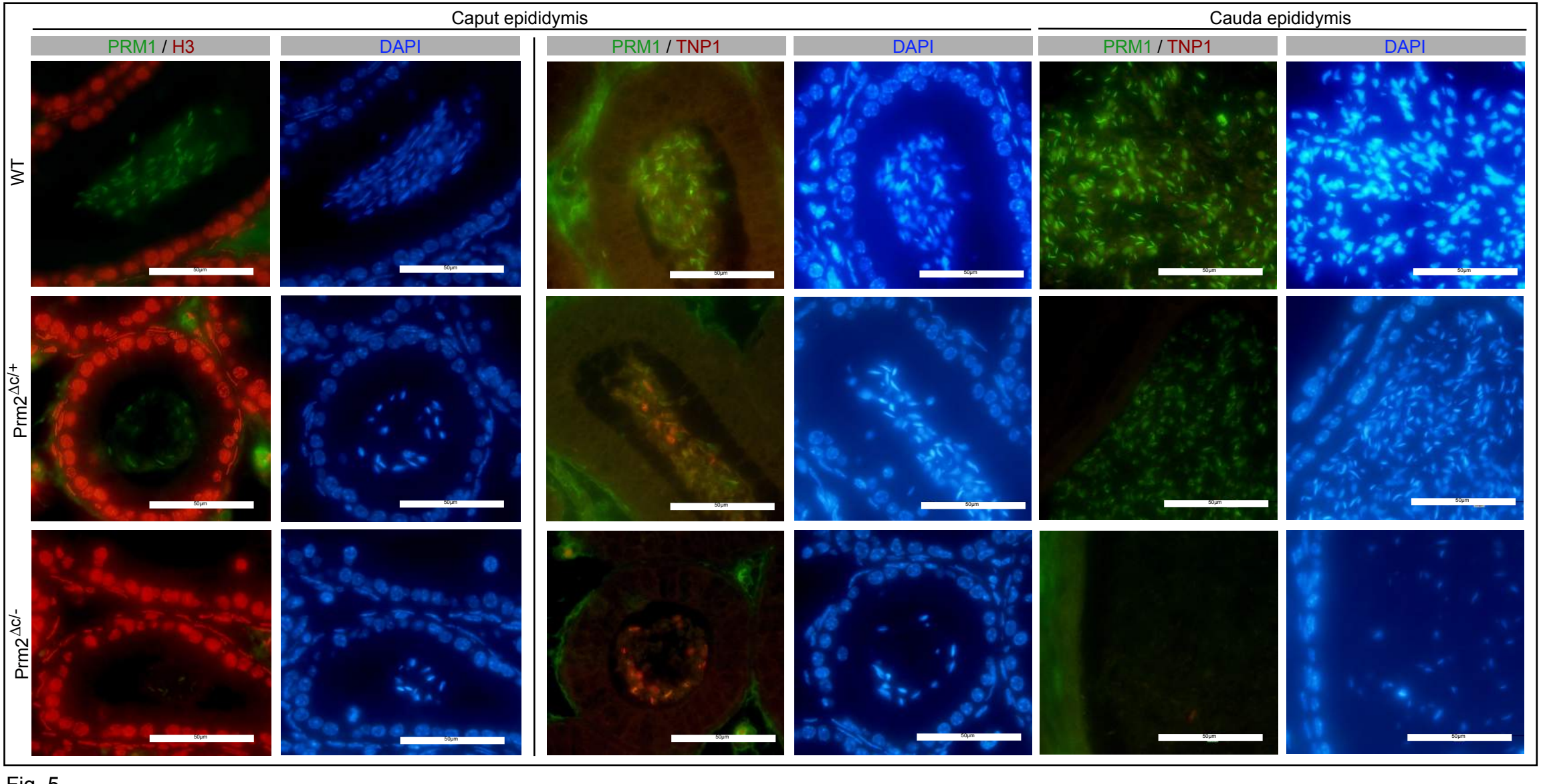

Fig. 5

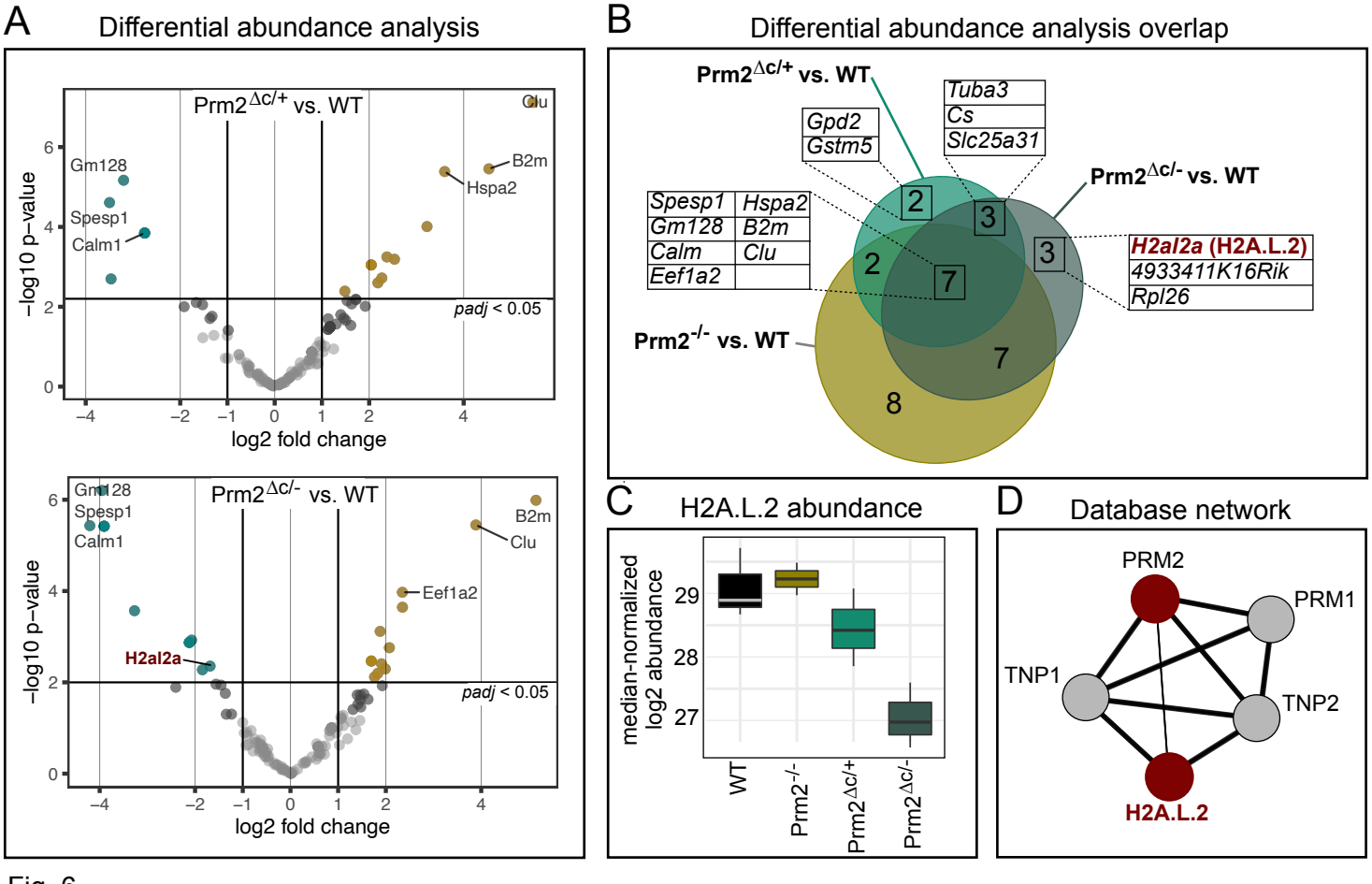
A
Differential abundance analysis
Prm2Δc/+ vs. WT
Clu
Gm128
B2m
Hspa2
Spesp1
Calm1
padj < 0.05
−log10 p−value
log2 fold change
Prm2Δc/- vs. WT
Gm128
Spesp1
Calm1
B2m
Clu
Eef1a2
H2al2a
padj < 0.05
−log10 p−value
log2 fold change
B
Differential abundance analysis overlap
Prm2Δc/+ vs. WT
Tuba3
Cs
Slc25a31
Gpd2
Gstm5
Prm2Δc/- vs. WT
Spesp1
Hspa2
Gm128
B2m
Calm
Clu
Eef1a2
H2al2a (H2A.L.2)
4933411K16Rik
Rpl26
Prm2-/- vs. WT
2
3
2
7
3
7
8
C
H2A.L.2 abundance
median-normalized log2 abundance
WT
Prm2-/-
Prm2Δc/+
Prm2Δc/-
D
Database network
PRM2
PRM1
TNP1
TNP2
H2A.L.2

Fig. 6

H2A.L.2 and PRM2 IHC

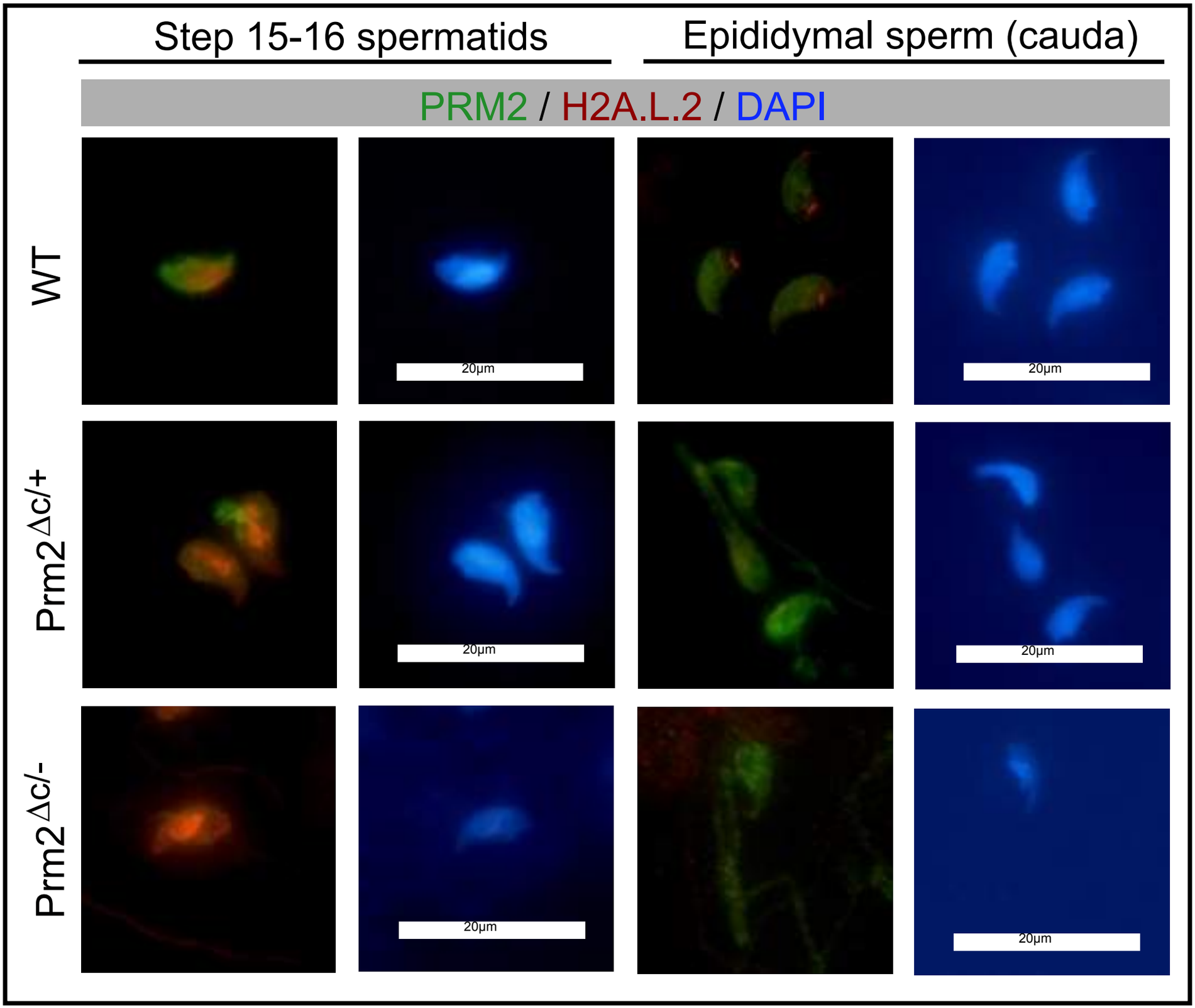

Fig. 7